

Numerical Study of the Effects of a Hot Obstacle on Natural Convection Flow Regimes

Z. Yahya^{1†} and A. M. Mahmoud²

¹Department of Physics, College of Science, Qassim University, Buraidah, 51452, P.O.Box 6644, Saudi Arabia

²Research Unit "New Energy Technologies and Thermo-fluid Systems nTEST", Department of Physics, Faculty of Science and Technology, Alaasriya University –Mauritania

†Corresponding Author Email: z.yahya@qu.edu.sa

(Received May 28, 2022; accepted November 17, 2022)

ABSTRACT

A numerical study was conducted for natural turbulent and laminar convection induced by a circular hot obstacle in two different positions, the heat obstacle is introduced at the inlet of the cylinder and inside the cylinder. To determine the effects of a circular hot obstacle on the regime of the thermosiphon flow generated by a heated cylindrical channel, we suggest a theoretical and numerical model using the Navier–Stokes equations and the finite volume method. An experimental apparatus was used for the validation of the numerical model. A comparison of the numerical and experimental results showed a good agreement in the global flow behavior. The temperature and vertical velocity profiles demonstrated the presence of a boundary-layer regime along the heated channel's wall in the absence of a hot obstacle and the presence of the hot obstacle at different positions. The introduction of the hot obstacle generates a significant modification of the evolution of the flow above the hot obstacle. The numerical simulation was conducted for a specific radius of the hot obstacle that ensures the existence in the laminar flow regime, and different Rayleigh numbers ($Ra=10^5$; 10^7 ; 10^8 ; 10^9 ; and 10^{10}). The flow rate, velocity, temperature and Nusselt number profiles were presented and discussed. The effects of the hot obstacle are presented in our results by two maxima of the vertical component of the velocity profile. The temperature profile at the entrance of the vertical cylinder is presented by the appearance of a maximum above the hot obstacle. As the cylinder height increases, the air temperature decreases. The vertical displacement of the obstacle upward induces a modification in the behavior of the dynamical flow. A CFD code was used to study the different natural convection regimes presented by three different form factors, including the critical regime with a form factor of $A=0.1$.

Keywords: Critical regime; Cylindrical hot wall; Numerical modeling; Thermosiphon flow; Navier–Stokes equations.

NOMENCLATURE

A	form factor ($A = \frac{2R}{H}$)	R_s	radius of the hot obstacle
a	cylinder diameter	Q	dimensionless flow rate
C_p	specific heat coefficient	T_0	the heated obstacle's temperature
g	the gravity acceleration	T_w	the temperature at the cylindrical wall of configuration A
H	cylinder height	T_w'	the temperature at the cylindrical wall of configurations B and C
H_s	vertical position of the heat obstacle	V_r, V_z	radial and longitudinal dimensionless velocity.
P	dimensionless pressure	α	the thermal diffusivity
r	dimensionless radial coordinate: $0 \leq r \leq \frac{R}{H} = \frac{A}{2} = \frac{0.3}{2} = 0.15$.	β	coefficient of thermal expansion
R	cylinder's radius	λ	thermal conduction coefficient
R^*	the ratio of the cylinder's radius to the hot obstacle's radius $R^* = R_s/R$	ν	kinematic fluid viscosity
Ra	Rayleigh number	(\cdot)	dimensional values

1. INTRODUCTION

The study of natural convection flow in a hot cylindrical channel is interesting from an applied point of view, such as in solar energy collection systems and the heating of electronic components. This type of flow can simulate many environmental systems, lowering the energy utilization and costs.

Furthermore, the applications of this study can also include fire forest and fires in buildings.

The structure of the natural convection flow induced by heated walls depends on the value of the Rayleigh number. A flow in a heated cylindrical tube of small dimensions having a low Rayleigh number is called a fully developed regime flow (Martin *et al.* 1991; Fujii *et al.* 1992). This regime is characterized by the absence of the development of a boundary layer along the walls, a transverse velocity of zero, and a vertical velocity independent of the tube height. The majority of the works investigating these flows are numerical or analytical studies. Using constant-flux or constant-temperature wall heating, the authors are mainly interested in determining the laws governing the heat transfer inside the tube ($Nu=f(Ra)$). For moderate values of the Rayleigh number, previous studies (Martin *et al.* 1991; Naffouti *et al.* 2016; Mahmoud and Yahya 2019) showed that the regime developed in the tubes divides into two zones. A first so-called heating zone begins from the inlet of the tube and reaches a height Z depending on the boundary conditions of the flow, and a second zone, called the zone of the fully established regime, starts from Z until the tube exit. In large Rayleigh number flows, the cylinder dimensions are large enough to promote the formation of a boundary layer along the hot wall. The air flow inside this wall is often defined as thermosyphon (Mahmoud 1998). The confinement of the fluid creates a pressure drop inside the cylinder. The resulting difference in air pressure due to Archimedes' force effect on the confined fluid causes the vertical entrainment of the cold fluid from the bottom of the cylinder.

Several works (AL Arbi *et al.* 1991; Maad and Belghuith 1989; Naffouti *et al.* 2016; Terekhov *et al.* 2016), have been devoted toward characterizing the heat transfer inside hot walls and toward determining the dynamics of the thermosyphon flow. They showed that at the system entrance, the vertical velocity is important in the central part, and that as the height increases, the velocity becomes increasingly intense near the wall and increasingly weak in the central part of the cylinder. If the hot walls are close to each other, this flow is characterized by the development of the boundary layer along the wall (Vorayos 2000; Pantokratoras 2006; Garnier 2015).

The presence of a hot obstacle in a low-temperature environment generates a natural convection flow that develops vertically under the effect of the Archimedes' forces (i.e., thermal plume). The first experimental studies (Rouse *et al.* 1952; Nakagome and Hirata 1976) devoted to these flows used point sources in the form of thin electrically heated wires, which showed that these turbulent flows are confined

to a conical region during their vertical evolution. To determine the turbulent structure of the flow, the choice of studies was oriented toward the use of a heat obstacle in the form of an electrically heated disc or a spherical cap. The studies of flows issuing from a hot disc (Maad 1995; Mahmoud 1998; Kapjor and Vantuch 2020) have shown the existence of two flow zones that characterize the vertical evolution of the flow. In the first zone, dominated by the Archimedes' forces, the profiles of velocities and temperature are Gaussian with a maximum situated on the axis. The second zone is one of similar profiles where the turbulence is fully developed. They demonstrated a radial widening of the velocity profile greater than that of the temperature.

Recently, works (Naffouti *et al.* 2016; Naffouti *et al.* 2018; Marzougui *et al.* 2022) have focused on the study of natural convection flows generated by rectangular sources in opened vertical channels. The flow regime studied is only the boundary layer regime. Transition to other regimes is not investigated.

The introduction of a hot obstacle at the entrance of a thermosyphon flow, generated by hot vertical cylindrical walls, can cause major modifications of the flow structure. This situation allows the superposition of two laminar and turbulent flows, the study of which will help better understand their interaction mechanisms.

Based on the above literature survey, natural convection flows highly depend on geometry and boundary conditions.

The novelty of our investigation is providing a specific geometry that presents the critical regime of the natural convection flow induced by a hot obstacle. The critical regime is the transition between the fully developed regime flow and the boundary-layer regime flow. The major difficulty in thermal natural convection in open or semi-open environments lies in estimating dynamic and thermal conditions, especially in the entrance area, which is the site of very complex and unpredictable phenomena, because they depend on the state of the fluid upstream. Furthermore, the effects of the position and diameter of the thermal source on the dynamic and thermal fields of the flow.

The Fortran code used in this work is based on the finite volume method and the Navier–Stokes equations. Our experimental measurements validated the CFD code.

The numerical resolution of the equations is realized for boundary conditions relating to three geometric configurations. One configuration is with boundary conditions of cylinder inlet with the absence of the hot obstacle. The other configurations are with boundary conditions with the presence of the hot obstacle in different positions ($Hs=0.05$).

A comparison of flow structure in these three configurations gives much information on the influence of a hot obstacle on the flow along the channel wall. The effects of dimensionless parameters, such as the Rayleigh number and form

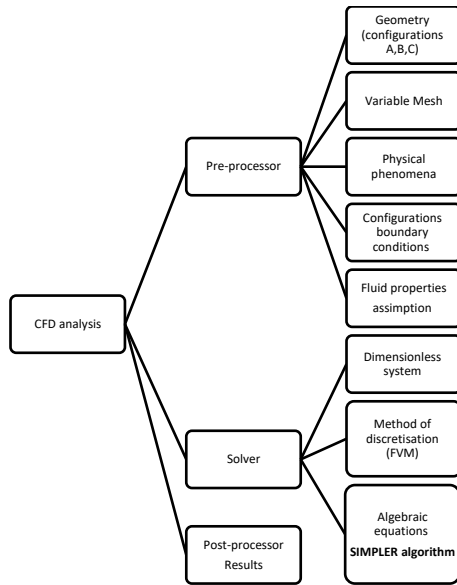


Fig. 1. CFD analysis Process.

factor, on the flow structure in the studied cases will also be investigated.

2. NUMERICAL MODEL

The CFD analysis contains three principal steps shown in Fig. 1.

The natural convection flow studied in this work is outlined for three configurations: a vertical heated cylinder (Fig. 2), a vertical cylinder with the presence of a hot obstacle at the cylinder inlet (Fig. 3), and a vertical cylinder with the presence of a hot obstacle inside the cylinder (Hs=0.05) (Fig. 4).

The studied flow is assumed to be two-dimension laminar, steady, and symmetric to the axis of the cylinder.

The fluid assumptions are:

- Newtonian
- viscous
- transparent
- the density in the equation of motion is variable and the other physical proprieties are constant.

Under the above assumptions, the dimensional equations that govern the heat transfers in the three configurations are as follows.

The continuity equation:

$$\frac{1}{r'} \frac{\partial}{\partial r'} (r' v'_r) + \frac{\partial}{\partial z'} (v'_z) = 0 \tag{1}$$

The r-momentum equation:

$$\left(v'_r \frac{\partial v'_r}{\partial r'} + v'_z \frac{\partial v'_r}{\partial z'} \right) = -\frac{1}{\rho_0} \frac{\partial p'}{\partial r'} + \nu \left[\frac{\partial}{\partial r'} \left(\frac{1}{r'} \frac{\partial}{\partial r'} (r' v'_r) \right) + \frac{\partial^2 v'_r}{\partial z'^2} \right] \tag{2}$$

The z-momentum equation:

$$\left(v'_r \frac{\partial v'_z}{\partial r'} + v'_z \frac{\partial v'_z}{\partial z'} \right) = -\frac{1}{\rho_0} \frac{\partial p'}{\partial z'} + \nu \left[\frac{1}{r'} \frac{\partial}{\partial r'} \left(r' \frac{\partial v'_z}{\partial r'} \right) + \frac{\partial^2 v'_z}{\partial z'^2} \right] + g\beta(T' - T_0) \tag{3}$$

The energy equation:

$$\rho_0 c_p \left[v'_r \frac{\partial T'}{\partial r'} + v'_z \frac{\partial T'}{\partial z'} \right] = \lambda \left[\frac{1}{r'} \frac{\partial}{\partial r'} \left(r' \frac{\partial T'}{\partial r'} \right) + \frac{\partial^2 T'}{\partial z'^2} \right] \tag{4}$$

The dimensional flow rate is given by:

$$Q' = 2\pi \int_0^R \rho' r' v'_z dr' \tag{5}$$

Using characteristic quantities:

$$v_0 = \frac{\alpha Ra^{0.5}}{H}, p_0 = \rho \cdot (v_0)^2; r = \frac{r'}{H}; z = \frac{z'}{H};$$

$$v_r = \frac{v'_r}{v_0}; v_z = \frac{v'_z}{v_0}; T = \frac{T' - T_0}{T_s - T_0} \text{ and } P = \frac{P' - P_0}{\rho_0}$$

Dimensionless Form of Continuity:

$$\frac{1}{r} \frac{\partial}{\partial r} (r v_r) + \frac{\partial}{\partial z} (v_z) = 0 \tag{6}$$

Conservation of r-momentum in Dimensionless Form:

$$\left(v_r \frac{\partial v_r}{\partial r} + v_z \frac{\partial v_r}{\partial z} \right) = -\frac{\partial p}{\partial r} - \frac{Pr Ra^{-0.5}}{r^2} v_r + Pr Ra^{-0.5} \cdot \left[\frac{\partial}{\partial r} \left(\frac{1}{r} \frac{\partial}{\partial r} (r v_r) \right) + \frac{\partial^2 v_r}{\partial z^2} \right] \tag{7}$$

Conservation of z-momentum in Dimensionless Form:

$$\left(v_r \frac{\partial v_z}{\partial r} + v_z \frac{\partial v_z}{\partial z} \right) = -\frac{\partial p}{\partial z} + Pr Ra^{-0.5} \cdot \left[\frac{1}{r} \frac{\partial}{\partial r} \left(r \frac{\partial v_z}{\partial r} \right) + \frac{\partial^2 v_z}{\partial z^2} \right] + Pr \cdot T \tag{8}$$

Dimensionless Form of the Energy Equation:

$$\left(v_r \frac{\partial T}{\partial r} + v_z \frac{\partial T}{\partial z} \right) = \left[\frac{1}{r} \frac{\partial}{\partial r} \left(r \frac{\partial T}{\partial r} \right) + \frac{\partial^2 T}{\partial z^2} \right] \tag{9}$$

where

$$Ra = \frac{g \cdot \beta \cdot (T_s - T_0) \cdot H^3}{\alpha \cdot \nu} \text{ and } Pr = \frac{\nu}{\alpha}$$

the dimensionless flow rate:

$$Q = 2\pi \alpha \rho_0 \cdot H \cdot Ra^{0.5} \int_0^{0.5A} \rho r v_z dr \tag{10}$$

The Nusselt number is given by:

$$Nu(z) = \frac{E_{v2} H}{(T_w - T_0) \lambda} \text{ were } E_{v2} \text{ is the heat flux} \tag{11}$$

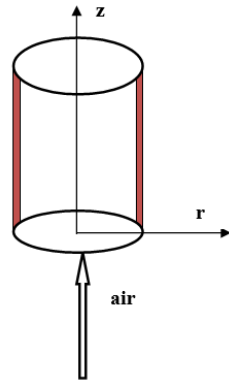


Fig. 2. Configuration (A). Vertical channel with heated walls.

2.1 Boundary conditions for natural convection flow inside a thermosiphon (Configuration A)

- At the wall

For viscous flow, the velocity at the wall is zero due to no-slip condition

$$\text{at } r = R; v_r(R, z) = v_z(R, z) = 0$$

In addition, the temperature at the wall is fixed

$$T(R, z) = T_w$$

- Axisymmetric boundary conditions

$$\text{at } r = 0 \frac{\partial v_r(0,z)}{\partial r} = \frac{\partial v_z(0,z)}{\partial r} = 0; \frac{\partial T(0,z)}{\partial r} = 0$$

- Inlet boundary

At the entrance of the channel, there is no radial velocity.

$$\text{at } z = 0; v_r(r, 0) = \frac{\partial v_z(r,0)}{\partial z} = 0; T(r, 0) = T_0$$

$$v_z(r, 0) = V_e$$

where V_e is the solution of the equation below:

$$-Pr.Ra^{-\frac{1}{2}} \frac{1}{r} \frac{\partial}{\partial r} \left(r \frac{\partial v_e}{\partial r} \right) = 1 \text{ (Le Quéré et al. 2004).}$$

- Outlet 'free plume'

At the outlet of the channel, the flow is fully developed, so the gradients for all the flow variables are zero.

$$\text{at } z = H; \frac{\partial v_r(r,H)}{\partial z} = \frac{\partial v_z(r,H)}{\partial z} = \frac{\partial p(r,H)}{\partial z}; \frac{\partial T(r,H)}{\partial z} = 0$$

2.2 Boundary Conditions for Natural Convection Flow Inside a Vertical Cylinder with a Hot Obstacle at the Entrance (Configuration B)

The same boundary conditions as in Configuration A are applied in Configuration B, except for the entrance and the at the wall, where:

$$\text{at } 0 \leq r \leq R_s; v_z(r, 0) = v_r(r, 0) = 0$$

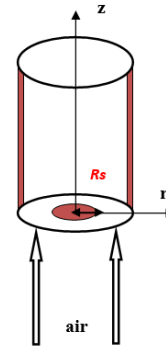


Fig. 3. Vertical channel with a hot obstacle at the entrance - Configuration (B).

$$T(r, 0) = T_s$$

$$\text{at } R_s \leq r \leq 0.5A, v_r(r, 0) = \frac{\partial v_z(r,0)}{\partial z} = 0$$

$$T(r,0) = T_0$$

$$\text{at the wall } T(R, z) = T_w'$$

where: R_s is the radius of the hot obstacle.

$$A = \frac{2R}{H} \text{ is the form factor}$$

2.3 Boundary conditions for a vertical cylinder with a hot obstacle at $H_s=0.05$ (Configuration C)

The same boundary conditions as in Configuration B are applied to the Configuration(C), except for the entrance boundary conditions, where

- Inlet boundary

$$\text{at } z = 0; v_r(r, 0) = \frac{\partial v_z(r,0)}{\partial z} = 0; T(r, 0) = T_0$$

$$\text{at } z=H_s; 0 \leq r \leq R_s; v_z(r, H_s) = v_r(r, H_s) = 0; T(r, H_s) = T_s$$

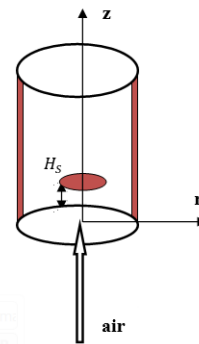


Fig. 4. Vertical cylinder with a hot obstacle at $H_s=0.05$ - Configuration(C).

$$\text{at } R_s \leq r \leq 0.5A \quad , \quad v_r(r, Hs) = \frac{\partial v_z(r, Hs)}{\partial z} = 0;$$

$$T(r, Hs) = T_0$$

3. EXPERIMENTAL APPARATUS

The experimental apparatus used for the numerical validation was composed of a circular disc with a diameter 7.5×10^{-2} m that was electrically heated at a constant and uniform temperature of 300°C. This obstacle was introduced at the inlet of the opened channel at its extremities, having a large diameter of 0.15 m and a height of 0.5 m. To decrease the thermal losses to the outside, the cylinder wall was thermally insulated. To facilitate the vertical and lateral entrainment of the air, the disc was mounted at an elevation of 0.85 m above the floor. The temperature of the air was measured with a precise measurement technique. The distribution of the temperature on the cylinder wall was measured at different heights by nine Al–Cr thermocouples. The relative variation in the temperature along the diameter of the hot disc was less than 2%.

The errors resulting from the probe calibration measuring studied velocities were situated in the interval $0.002 \leq \Delta U_e \leq 0.012$. For the air temperature, the calibration errors were within the interval $0.003 \leq \Delta T_e \leq 0.01$. Standard errors on the used thermocouples vary between 0.0075 and 0.022.

The mean temperature and velocity fields were measured via a hot-wire anemometry technique that used the variation in the electric resistance of a platinum wire (having a diameter of 7.5 μ m and a length of 3 mm) with air temperature. The electrical resistance of the wire varied with the air velocity and temperature in the plume. Authors have showed that an electrical intensity of 1.2 mA allows the wire to be sensitive only to the air temperature, while an electrical intensity of 38 mA allows it to be sensitive to the air temperature and velocity. The velocity and temperature of the air were determined according to a probe calibration from the voltage across the probe. To conduct the measurements without disturbing the flow, the wire had to constant lyre main perpendicular to the ascending flow. Thus, the probe was placed vertically to the flow inside the cylinder. At low flow frequencies, the thermal inertia of the wire (the time constant of the wire was of the order of 1 ms) did not introduce any measurement errors to the temperature and velocity of the air. The errors resulting from the probe calibration were lower than 1%.

To determine the dynamics and the thermal fields of the flow, a computer-controlled displacement system was performed in two directions. The minimal displacement in the radial direction was 2×10^{-5} m, whereas along the height it was 2×10^{-3} m.

For statistical data processing, a device equipped with a digital card for data recording acquired and recorded instantaneous values of the signal at intervals of 10 ms. The mean values of the temperature and velocity of the air were determined by a statistical treatment of the obtained results.

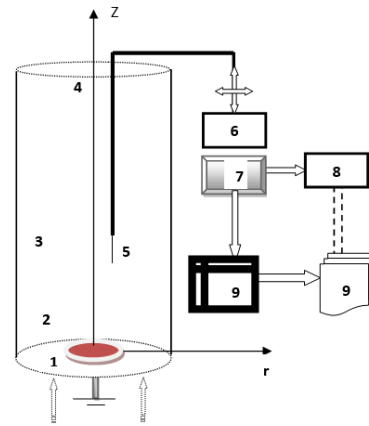


Fig. 5. Experimental device. 1 Hot disc; 2 Cylinder's inlet; 3 Al-Cr thermocouples 4 Cylinder's exit; 5 Hot wire 6 Displacement system 7 Data logger; 8 Data storage 9 Statistical data processing and Results storage

Because of the sensitivity of the flow to environmental conditions, the experiments were conducted in a calm place. The experimental device was mounted inside a closed room, whose temperature indicated a relative variation that remained below 5%.

4. EXPERIMENTAL VALIDATION OF THE NUMERICAL MODEL

The experimental validation of the numerical model was conducted with a geometric configuration having same dimensions, same boundary conditions and same Rayleigh number. A comparison of the results was made for the corresponding Ra number ($Ra = 0.7 \times 10^9$) and aspect ratio ($R^* = 0.2$).

The velocity and temperature profiles given by the numerical model were compared with the experimental results. Fig. 6 and Fig. 7 show that the numerical results have a tendency similar to the experimental measurements. Figure 6 represents a comparison of the velocity profile provided by the numerical model and experimental results at the entrance system. A qualitative comparison of these profiles shows an excellent agreement in the general thermal behavior of the flow. The differences that are observed between the profiles above the hot source can be explained by the effects of the strong mixture of fresh and hot air layers caused by the formation of rotating rolls, as was noted in other experimental works (Davis and Perona 1971). Figure 7 illustrates the comparison of the temperature profile obtained by the numerical model and the experiment at the system entrance. One can notice that the numerical results are in good agreement in terms of the general flow structure. Therefore, the average flow is well reproduced by the numerical model. However, we notice an underestimation of the vertical velocity profiles compared to the experimental results. This underestimation can be explained by the effects of wall heating by the hot source, which help intensify

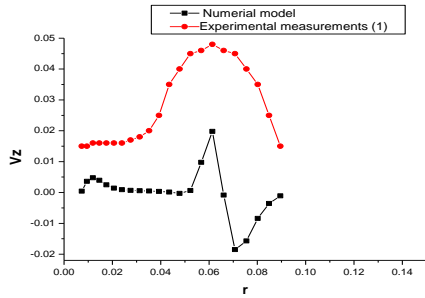


Fig. 6. Comparison of V_z versus r obtained by the numerical model and the experiment near the system entrance.

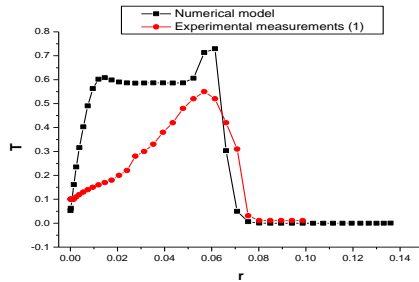


Fig. 7. Comparison of T versus r obtained by the numerical model and the experiment near the system entrance.

fluid suction at the system entrance. The flow visualization (Davis and Perona 1971; Mahmoud 1998) shows the existence of a zone of the strong mixing of the fluid with the formation of rotating rolls above the hot source and a return flow at the vicinity of the wall. All these effects are not considered by the laminar numerical model.

5. RESULTS AND DISCUSSIONS

Steady, laminar, and two-dimensional natural convection flow is modeled mathematically and numerically. The results are obtained using a FORTRAN code.

Using the SIMPLER algorithm, the velocity–pressure coupling is resolved.

The results are obtained for configurations A, B, and C) to investigate the flow behavior in a heated cylinder and a vertical cylinder with the presence of a hot obstacle in two positions.

The results are relative to the air and correspond to a Prandtl number equal to 0.7 and for different form factors ($A = 0.05; 0.1; 0.15; \text{ and } 0.3$) and different Rayleigh numbers ($Ra = 10^{+5}; 10^{+7}; 10^{+8} \dots$).

In Configurations B and C, the ray ratio of the heat source to the cylinder corresponds to $R^* = 0.2$.

The convergence criterion in the Fortran code is given by $\epsilon_F = 10^{-4}$.

We carry out different numerical tests to test the grid independency in different cases ($R^* = 0.2; \dots 0.46$) and ($Ra = 10^{+5}; 10^{+7} \dots$) starting from a rather

coarse mesh 101×201 towards a more refined mesh 501×501 until the refinement no longer affects the results.

Figure 8 (a,b) shows that the mesh (501×501) of this study is characterized by:

- high accuracy
- an acceptable volume of computation.

5.1 Natural Convection Flow Inside a Heated Cylindrical Channel (Configuration A)

Figure 9 (a, b, and c) shows the radial distribution of the horizontal component of the air velocity at different altitudes and form factors. For the lowest form factor ($A=0.05$), Fig. 9a indicates a zero-radial velocity at different altitudes, indicating an established regime inside the cylinder. We find the same result in the case of heated plates with small spacing (Maad 1995). An onset of change in the flow regime is observed from the form factor ($A=0.1$) where the radial velocity begins to appear (Fig. 9b). The boundary-layer regime is clearly noted for the form factor ($A=0.3$) where the air velocity remains constant in the central part of the cylinder and the radial velocities appear at all altitudes (Fig. 9c). The profiles show that the air tends to move from the central part of the cylinder toward the hot walls. This horizontal movement of the air, which is of low intensity compared to the vertical movement, becomes increasingly important with increasing cylinder radius. This behavior is confirmed by the radial evolution of the vertical component of the velocity at different altitudes (Fig. 10a, b, and c).

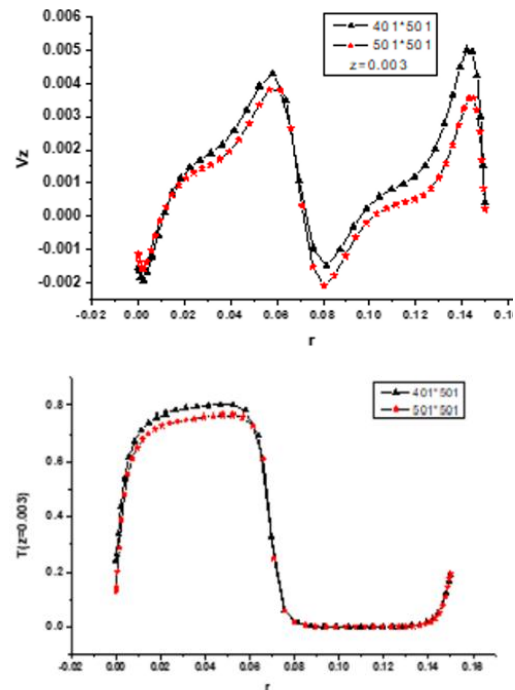


Fig. 8. Grid independency.

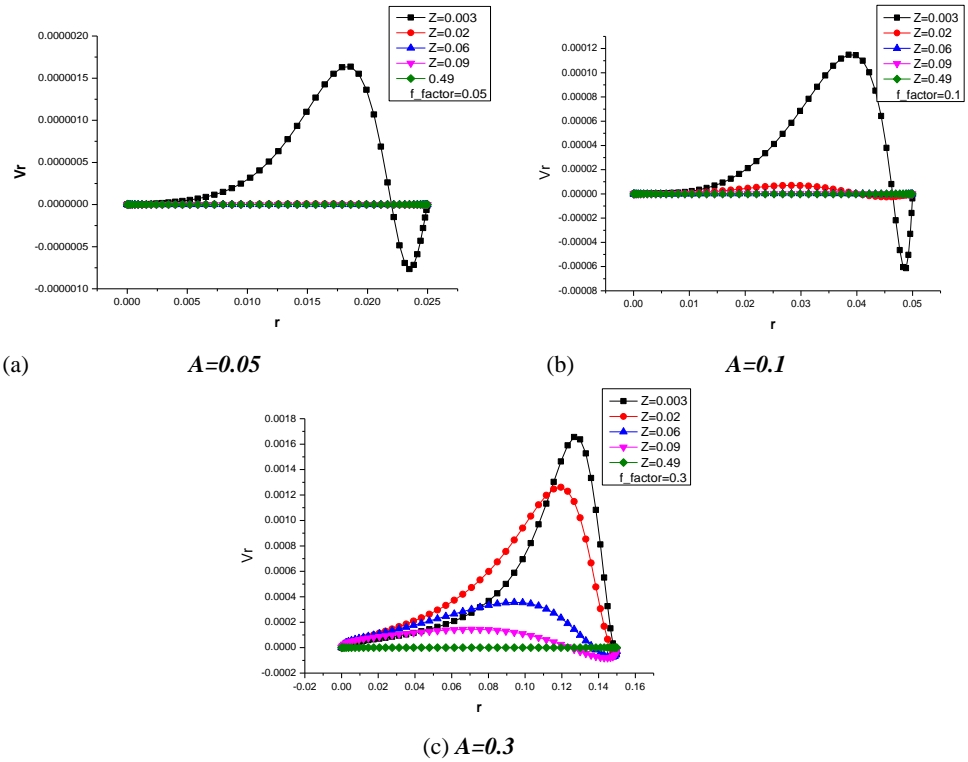


Fig. 9. Radial dimensionless velocity for three form factors (Configuration A).

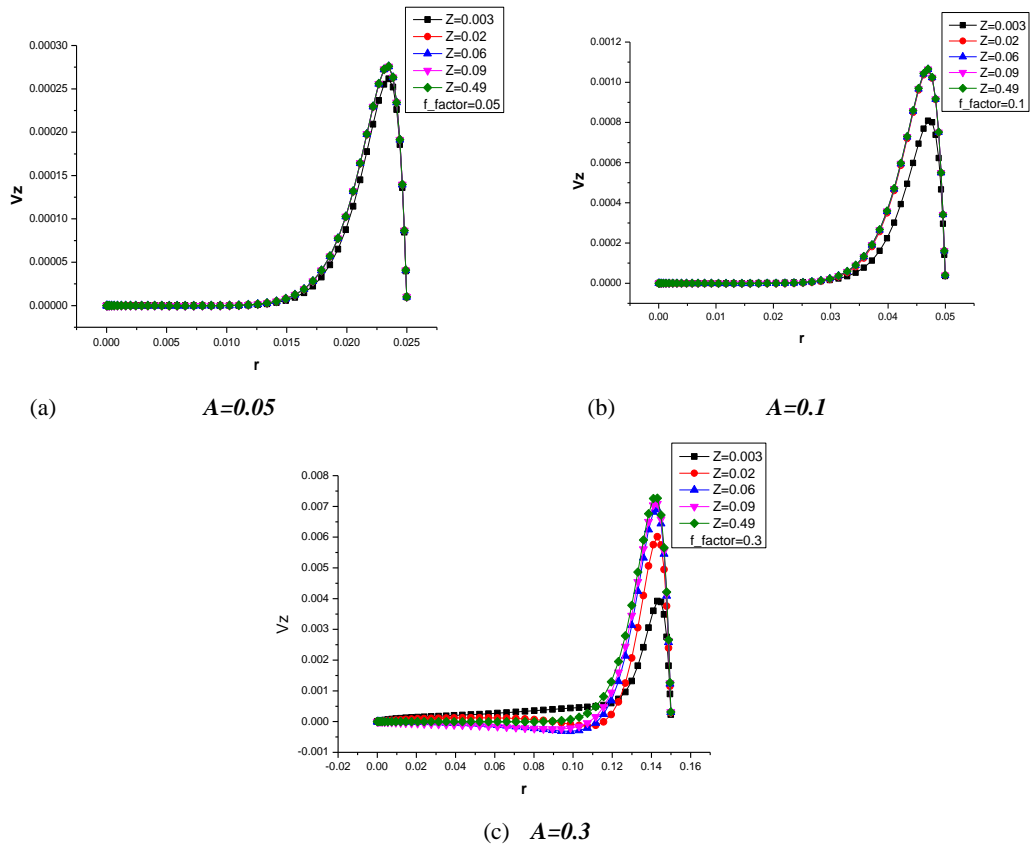


Fig. 10. Longitudinal dimensionless velocity for three form factors (Configuration A)

Following the confinement of the air inside the cylinder, the driving pressure drop causes an entrainment of the cold air from below, which will be used to supply the boundary layers along the hot

walls. As the height Z increases, the vertical flow becomes increasingly intense near the wall and increasingly weaker in the central part of the cylinder (i.e., the thermosiphon flow). The radial evolution of

the flow temperature at different altitudes seems to be independent of the weak variations in the form factor; a slight temperature variation is observed in the boundary-layer regime for $A=0.3$ (Fig. 11a, b, and c).

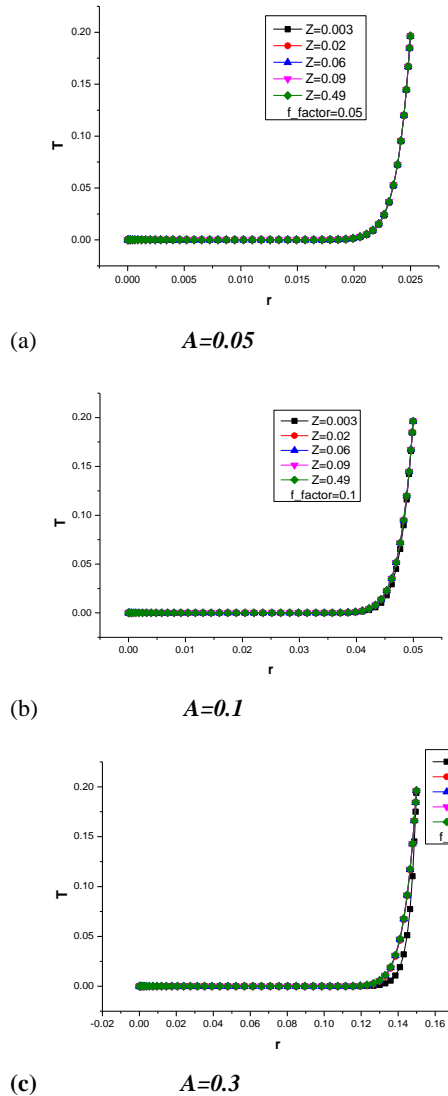


Fig. 11. Dimensionless temperature for three form factors (Configuration A).

5.1.1 Effects of Rayleigh number on a thermosiphon flow for $A=0.3$ (Configuration A)

In the boundary-layer regime, the air entrainment by the hot wall becomes increasingly important when the Rayleigh number increases (Fig. 12a, b).

Figure 13 shows the influence of the Rayleigh number on the Nusselt number. The relationship between these two numbers follows an exponential evolution. The Nusselt number is almost constant for low Rayleigh numbers, while it increases sharply for high Rayleigh numbers.

Figure 14 shows the radial evolution of the dimensionless flow rate at three altitudes. These

profiles show that the flow rate is high near the hot walls and remains low in the cylinder center.

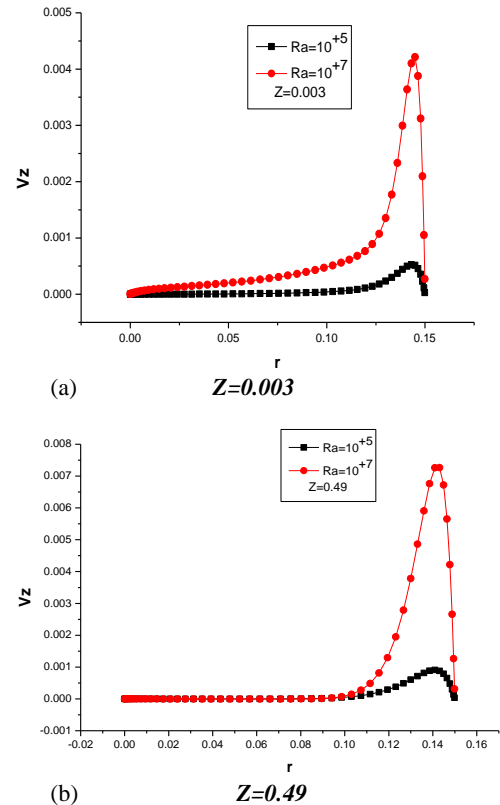


Fig. 12. Influence of Rayleigh number on the longitudinal dimensionless velocity (Configuration A).

5.2 The Obstacle–Cylinder Interaction flow induced by a Hot Obstacle placed at the cylinder inlet (Configuration B)

In Configuration B, the hot obstacle is placed at the cylinder inlet to determine the behavior of the resulting flow for different form factors.

5.2.1 Effects of a cylindrical shape on an Obstacle–Cylinder Interaction flow (Configuration B)

The interaction between the hot obstacle and the flow inside the cylinder does not seem to affect the flow regimes. The established regime always appears at the same form factor ($A=0.05$) (Fig. 15a) and the transition to the boundary-layer regime is obtained by the form factor ($A=0.1$) (Fig. 15b). The boundary-layer regime appears when the distance between the walls is large ($A=0.3$) (Fig. 15c). In the boundary-layer regime ($A=0.3$), a significant lateral air at the system inlet is caused by the presence of the hot obstacle, as seen in Fig. 15c.

The radial evolution of the longitudinal dimensionless velocity for various form factors is illustrated in Fig. 16 (a, b, and c). At the system inlet

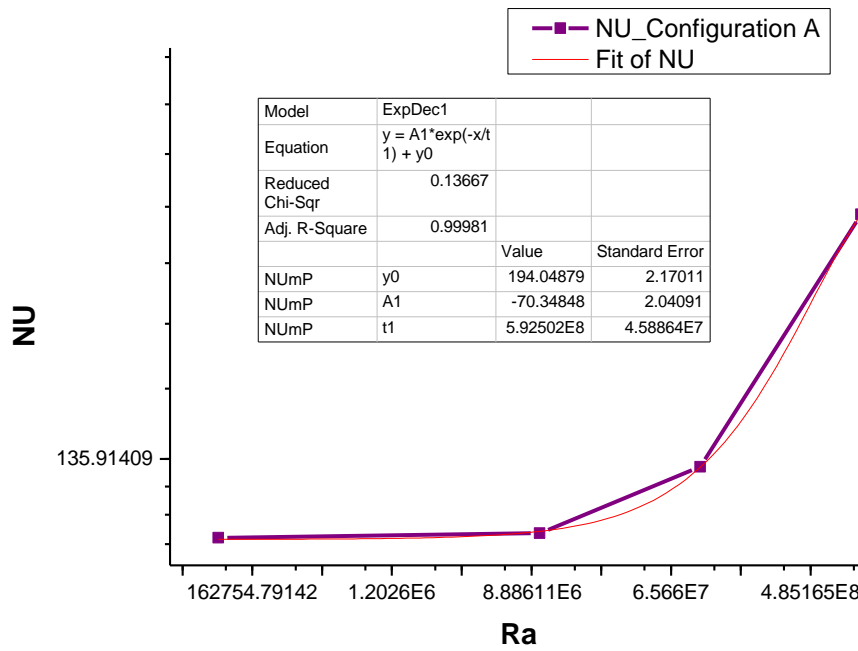


Fig. 13. Rayleigh number's impact on the Nusselt number (Configuration A).

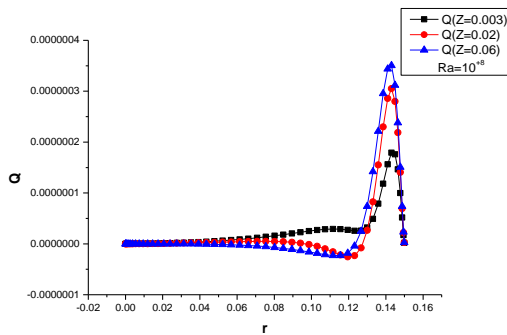


Fig. 14. Dimensionless flow rate at different altitudes (Configuration A).

for the three form factors, the impact of the hot obstacle is noticeable. The established regime ($A=0.05$) is characterized by similar profiles except at the entrance (Fig. 16.a). The boundary layer regime ($A=0.3$) is characterized by the presence of velocity maxima near the axis and at the system entrance (Fig. 16.c), which is confirmed by the experimental results and by other studies (Naffouti *et al.* 2010).

The impact of the hot obstacle on the air temperature is considerable at the channel inlet for the three form factors (Fig. 17.a.b.c).

5.2.2 Effects of Rayleigh number on Obstacle–Cylinder Interaction flow (Configuration B)

The influence of Rayleigh number on the longitudinal dimensionless velocity at the inlet and at the exit of the cylinder is shown in Fig. 18a and b. The maxima observed in the vicinity of the axis and at the wall increase with the Rayleigh number, which

means that the effects of the hot obstacle are clearly noted when the Rayleigh number is elevated.

The development of the Nusselt number with the Rayleigh number follows an exponential variation as illustrated in Fig. 19, as was indicated in the case without an obstacle (Fig. 13).

The radial development of the dimensionless flow rate at three altitudes inside the cylinder is illustrated in Fig. 21. This figure shows that the flow in the vicinity of the hot wall increases with altitude, while it remains low in the center of the cylinder.

5.3 Effects of heat source position on Obstacle–Cylinder interaction flow (Configuration C)

The radial evolution of the radial dimensionless velocity at different altitudes and $H_s=0.05$ is presented in Fig. 22. The obstacle is introduced at a distance $H_s=0.05$ from the entry of the cylinder. The profiles show that below the hot obstacle, the radial velocity is relatively low. It increases at the level of the obstacle position, and then decreases in the upper part of the cylinder.

Figure 23 illustrates the longitudinal dimensionless velocity at various heights and for the obstacle position $H_s=0.05$. It should be noted that the air longitudinal velocity in the vicinity of the obstacle increases with height to reach a maximum at the level of the obstacle position and then decreases at higher altitudes. At the same position H_s , the radial evolution of the air temperature is shown in Fig. 24. This figure clearly illustrates that the air temperature is affected only at the obstacle position, and it remains low at other altitudes.

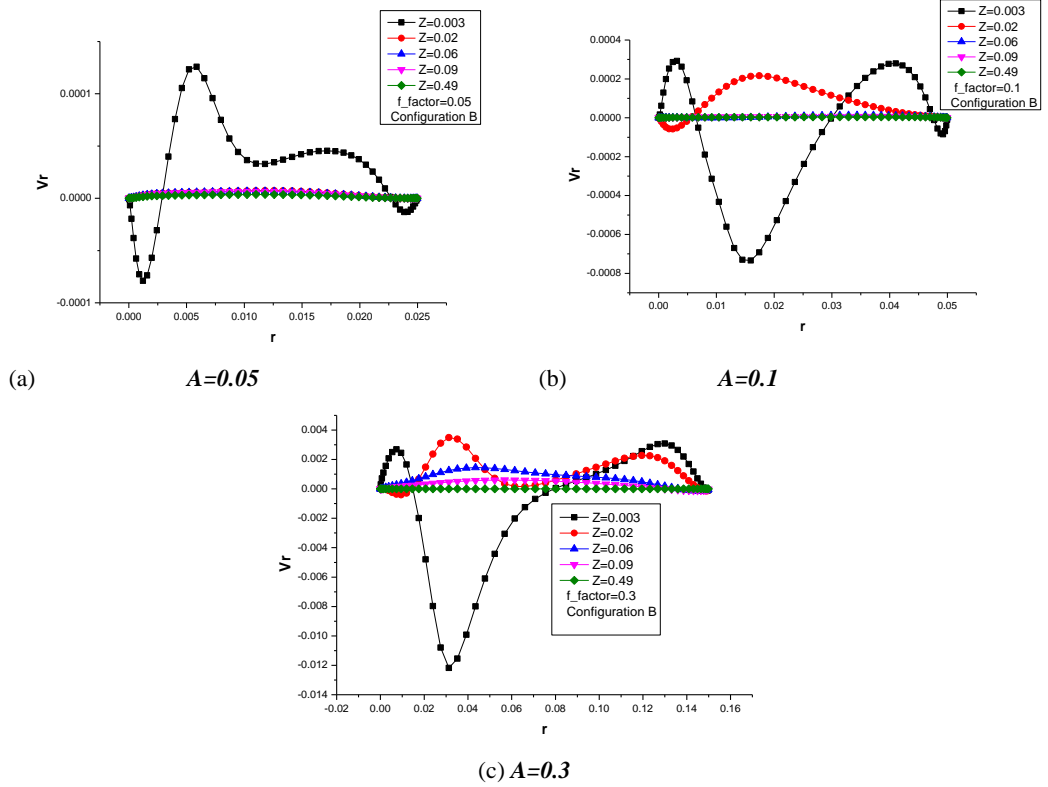


Fig. 15. Dimensionless radial velocity for various form factors (Configuration B).

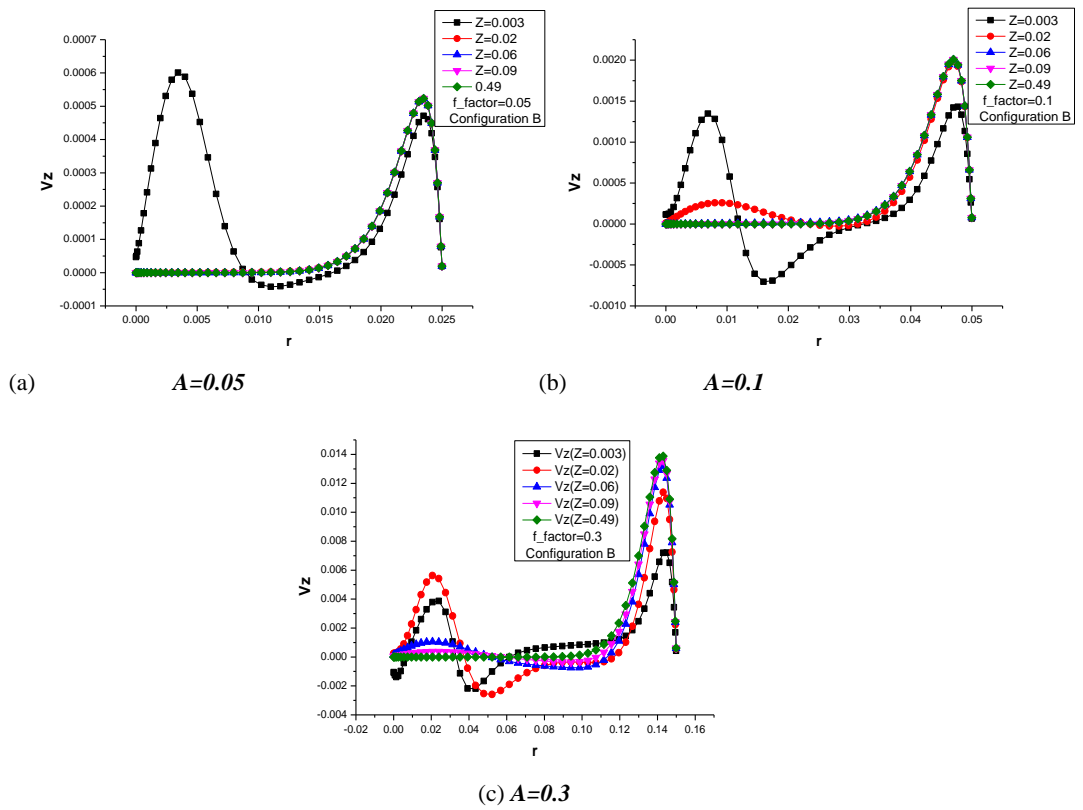


Fig. 16. Dimensionless longitudinal velocity for various form factors (Configuration B).

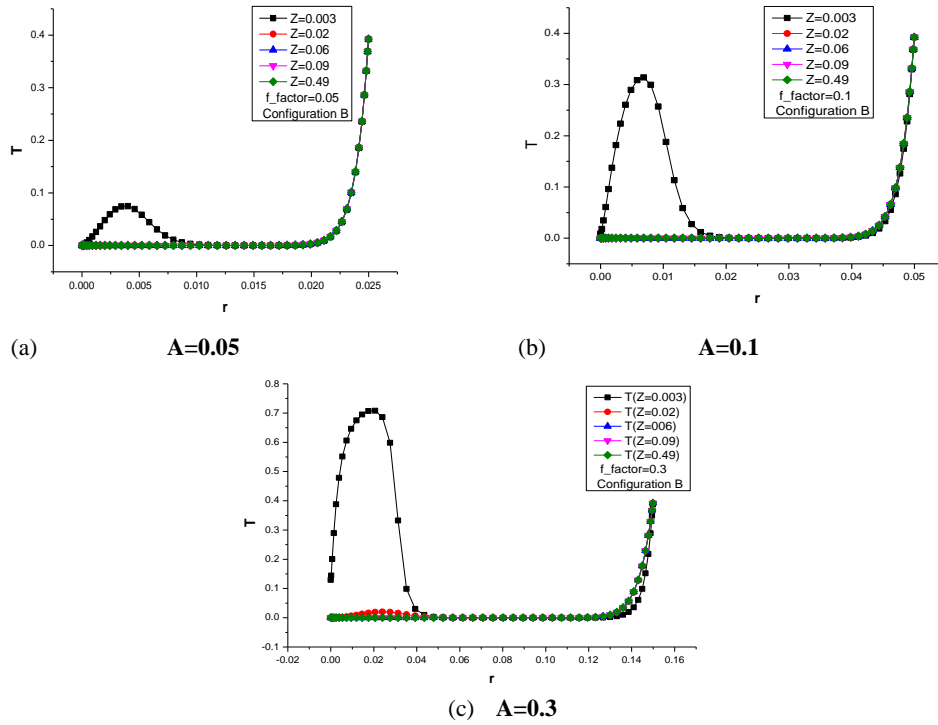


Fig. 17. Radial evolution of the dimensionless temperature for different form factors (Configuration B).

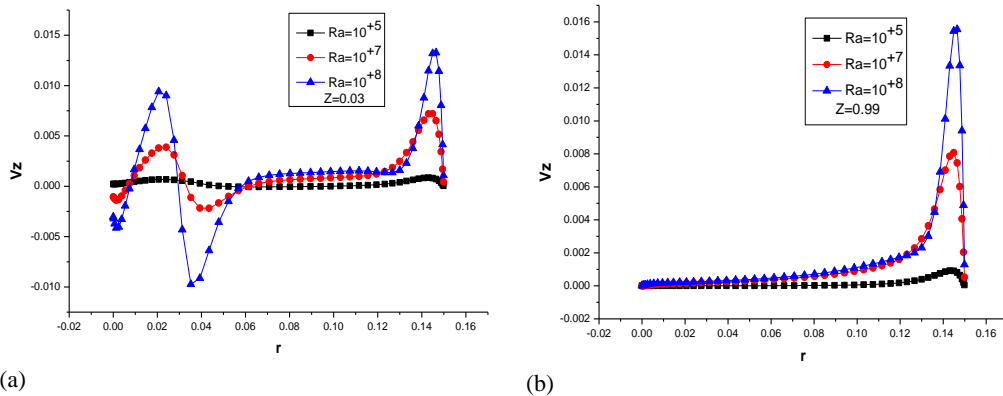


Fig. 18. Influence of Rayleigh number on the longitudinal dimensionless velocity (Configuration B).

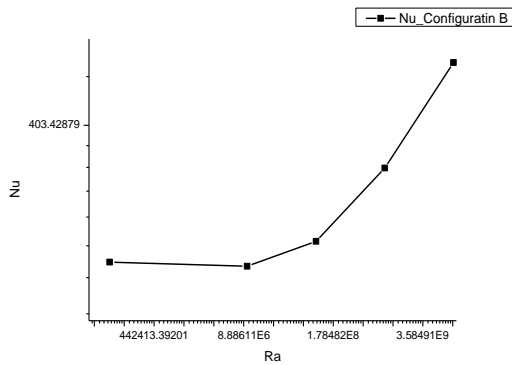


Fig. 19. Rayleigh number's impact on the Nusselt number (Configuration B).

The Rayleigh number's impact on the vertical component of the air velocity is clearly manifested at the inlet (Fig. 25a) and at the exit of the cylinder (Fig. 25.b). The air entrainment in the vicinity of the cylindrical wall and at the level of the obstacle axis becomes increasingly important with the increase in Rayleigh number.

The Rayleigh number's impact on the Nusselt number is represented in Fig. 26. This variation follows the same profile as in the previous configurations (A and B).

The radial evolution of the dimensionless flow rate at different altitudes is given in Fig. 27. The profiles show that the flow rate at the flow inlet is weak into the central part of the cylinder and increases at the vicinity of the hot wall; however, it reaches a

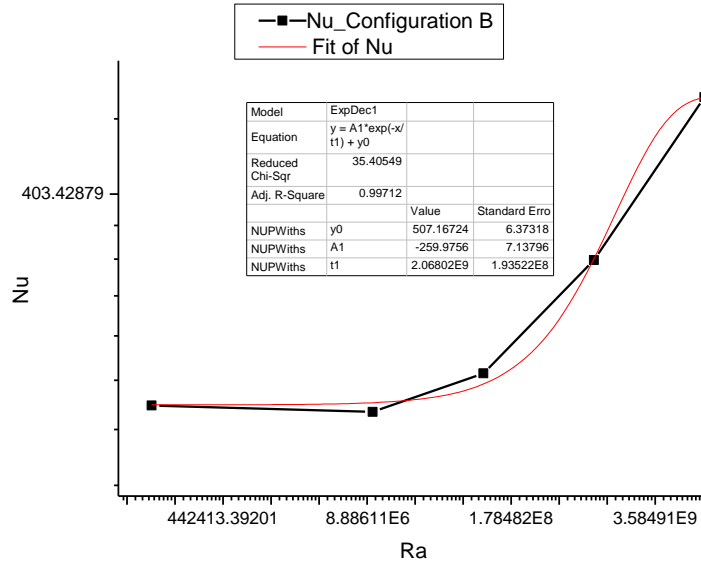


Fig. 20. The fit of the Rayleigh number's impact on the Nusselt number (Configuration B).

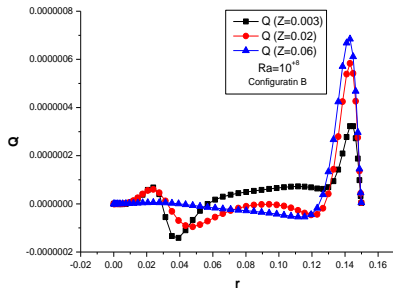


Fig. 21. Radial evolution of the dimensionless flow rate (Configuration B).

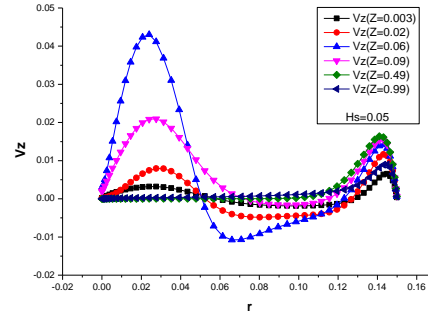


Fig. 23. Longitudinal dimensionless velocity at different altitudes (Configuration C).

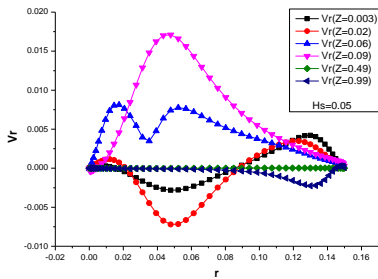


Fig. 22. Radial dimensionless velocity at different altitudes (Configuration C).

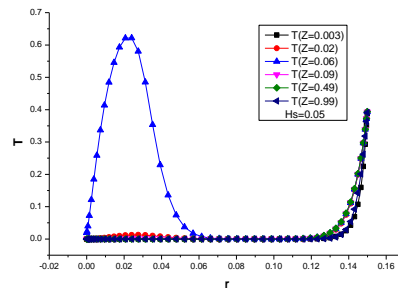
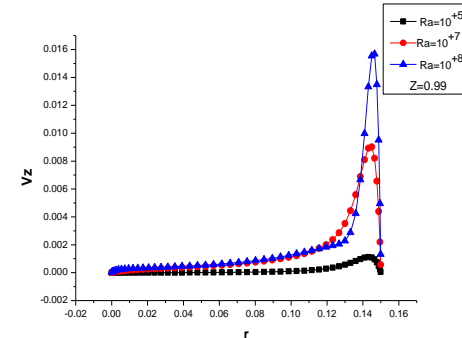
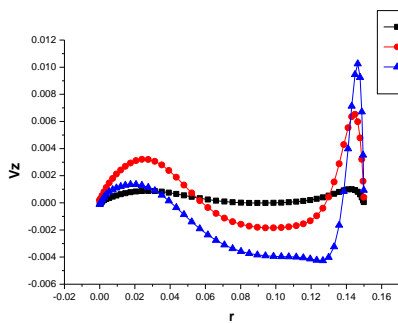


Fig. 24. Radial evolution of the dimensionless temperature (Configuration C).



(a) (b)
Fig. 25. Rayleigh number's impact on the longitudinal dimensionless velocity (Configuration C).

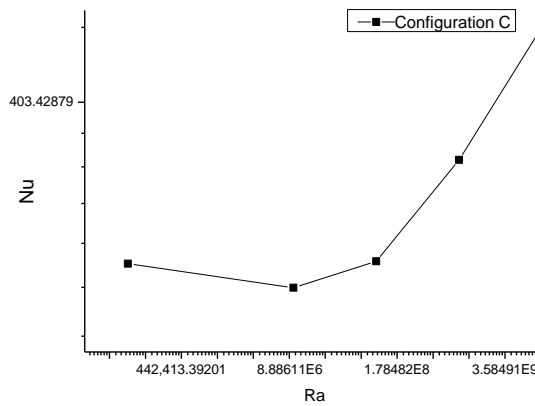


Fig. 26. Rayleigh number's impact on the Nusselt number (Configuration C).

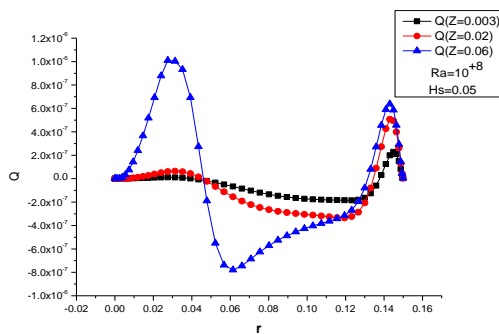


Fig. 27. Dimensionless flow rate at different altitudes (Configuration C).

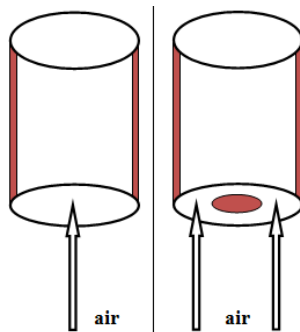


Fig. 28. Comparative Study Configuration (A): Thermosiphon – Configuration (B): Obstacle-Cylinder Interaction.

maximum at the level of the obstacle position and remains high in the vicinity of the wall. Thus, the influence of the hot obstacle starts from its height position.

5.4 Comparative study

5.4.1 Comparative study between configurations A and B

Figure 29(a, b) shows a comparison of the radial velocities in configurations A and B at two altitudes. At the system inlet (Fig. 29a), the lateral air entrainment caused by the hot obstacle is significant,

while the air attracted by the hot wall remains relatively low, which shows the dominant effect of

the obstacle on the flow. When the height increases, the radial air velocity profile appears at two maxima: one near the wall, and one located close to the obstacle axis (Fig. 29b).

A comparison of the longitudinal velocities in configurations A and B is shown in Fig. 30(a, b). At the heated cylinder inlet (Fig. 30a), the effects of the hot obstacle on the thermosiphon flow are reflected by a longitudinal air velocity that has two peaks close to the wall and the axis of the hot obstacle. As the cylinder height increases, the longitudinal air velocity keeps the same shape and greater intensity (Fig. 30b).

A comparison of the dimensionless temperature in configurations A and B is presented in Fig. 31(a, b). The air temperature at the cylinder inlet is affected by the hot obstacle, as illustrated by the appearance of a maximum close to the hot obstacle's axis (Fig. 31a), and the peak close axis flattens significantly, but the peak near the wall maintains elevated (Fig. 31b).

The Rayleigh number's impact on the Nusselt number in configurations A and B is illustrated in Fig. 32. The effects of the presence of the hot obstacle at the cylinder inlet are clearly noted by the considerable improvement in the Nusselt number.

A comparison of the radial evolution of the dimensionless flow rate into the two Configurations A and B is shown in Fig. 33(a, b). This figure shows that the flow in the vicinity of the hot wall increases with the presence of the hot obstacle at two altitudes. Above the hot obstacle, the flow rate is greater, which can be explained by the existence of air currents coming from the bottom of the cylinder to supply the flow.

5.4.2 Comparative study between configuration B and configuration C

Figure 35(a,b,c) presents a comparison between the radial dimensionless velocity in configurations B and C. At the system entrance, the lateral air entrainment

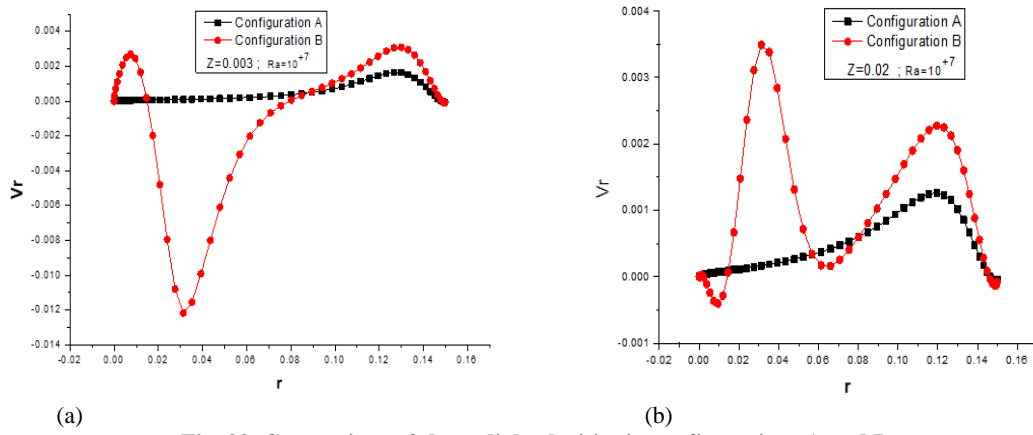


Fig. 29. Comparison of the radial velocities in configurations A and B.

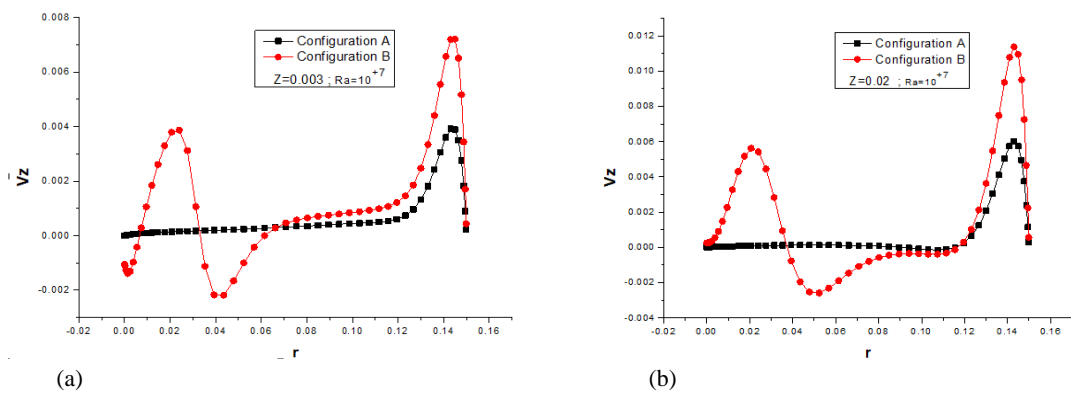


Fig. 30. Comparison of the longitudinal velocities in configurations A and B.

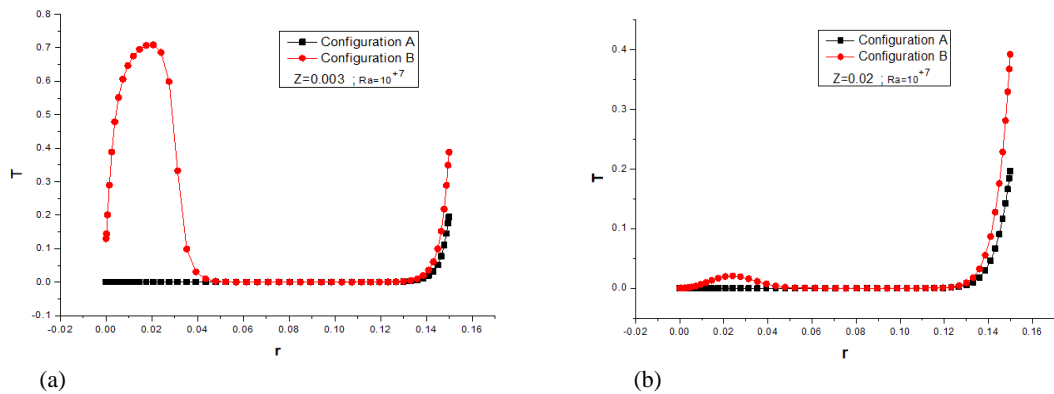


Fig. 31. Comparison of the dimensionless temperature in configurations A and B.

is intense in Configuration B due to the presence of the obstacle just at the entrance, whereas in Configuration C, the obstacle is located at height H_s from the entrance, which explains the absence of air entrainment in this region (Fig. 35a). A lateral air entrainment is observed at altitude $Z=0.02$ due to the presence of the obstacle at position H_s (Fig. 35b). At the level of the obstacle position H_s , the lateral air velocity appears in three extrema profile with two maxima—one in the vicinity of the axis, and the other at the obstacle border—and a minimum located at the mid-radius of the disc (Fig. 35c). This behavior can be explained by the existence of air currents coming from the system inlet to supply the flow above the hot obstacle.

Figure 36 shows a comparison of the longitudinal dimensionless velocity in configurations B and C. The behavior of the longitudinal air velocity at the system inlet changes when the obstacle is elevated (Fig. 36a). As the height increases, the vertical velocity profiles are identical near the wall and different in the center, with configuration C showing a higher maximum (Fig. 36b). At the level of obstacle position H_s , the vertical velocity presents a maximum near the axis vicinity, which is explained by the flow supply through this region (Fig. 36c).

Figure 37. presents a comparison between the dimensionless temperature in configurations B and

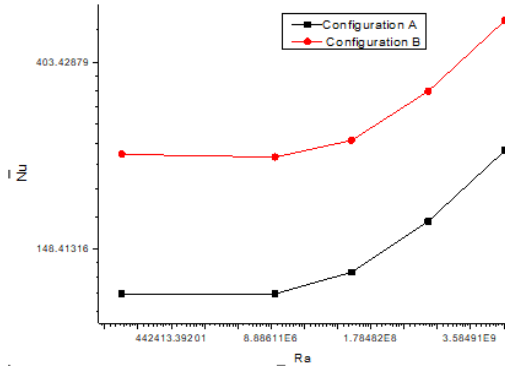


Fig. 32. Comparison of the Rayleigh number's impact on the Nusselt number in configurations A and B.

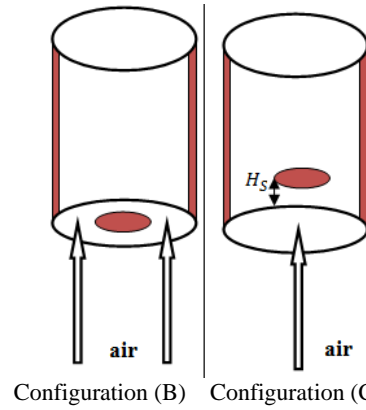
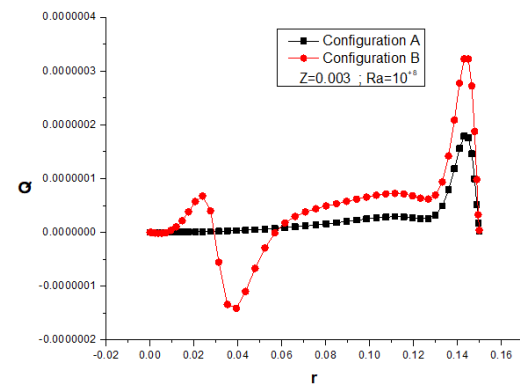
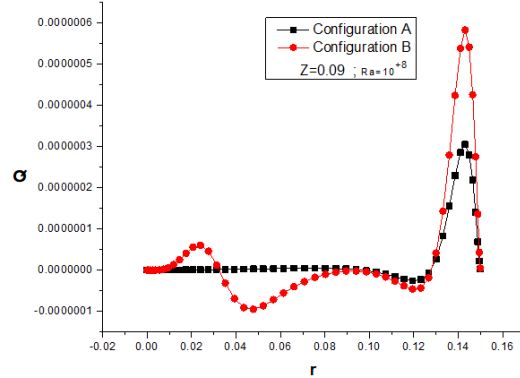


Fig. 34. Comparative Study Configuration (B): Obstacle-Cylindre Interaction $H_s=0$ – Configuration (C): Obstacle-Cylindre Interaction $H_s=0.05$.



(a)

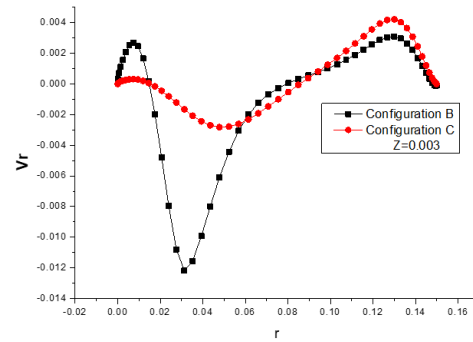


(b)

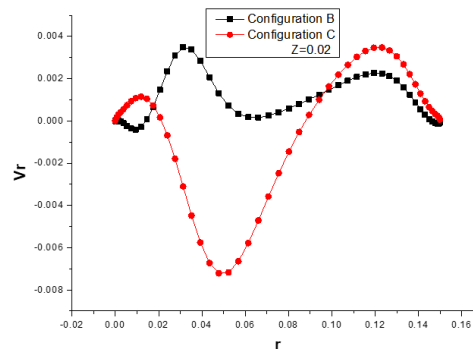
Fig. 33. Comparison of the Q versus r in configurations A and B.

C. According to the profiles, for all obstacle positions, the air temperature is at its highest close to the axis above the hot disc.

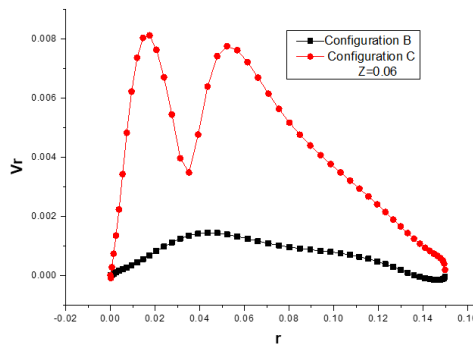
Figure 38 shows an improvement of the Nusselt number in configuration C at low Rayleigh numbers. A comparison of the dimensionless flow rate in configurations B and C is shown in Fig. 39. At the system entrance, Fig. 39(a) indicates that the flow rate is greater near the wall in both configurations. The flow rate remains higher at altitudes below the height of the obstacle position. Above the obstacle position H_s ($Z=0.06$), the flow rate is greater, which can be explained by the existence of air currents coming from the bottom of the cylinder to supply the flow.



(a)



(b)



(c)

Fig. 35. Comparison of the radial dimensionless velocity in configurations B and C.

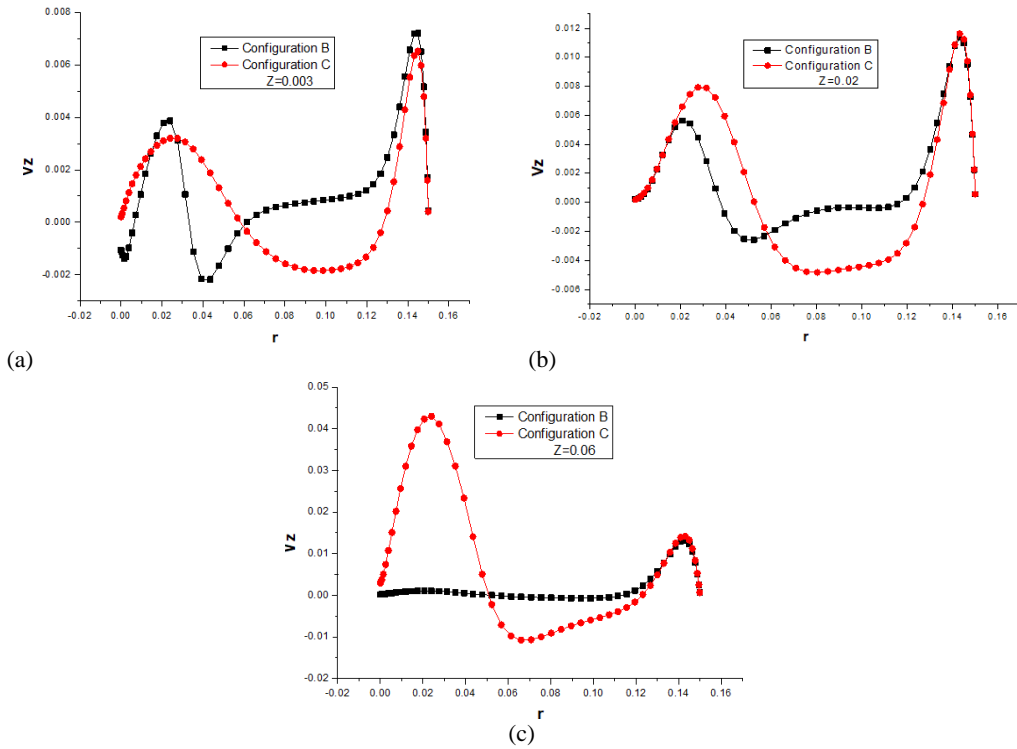


Fig. 36. Comparison of the longitudinal dimensionless velocity in configurations B and C.

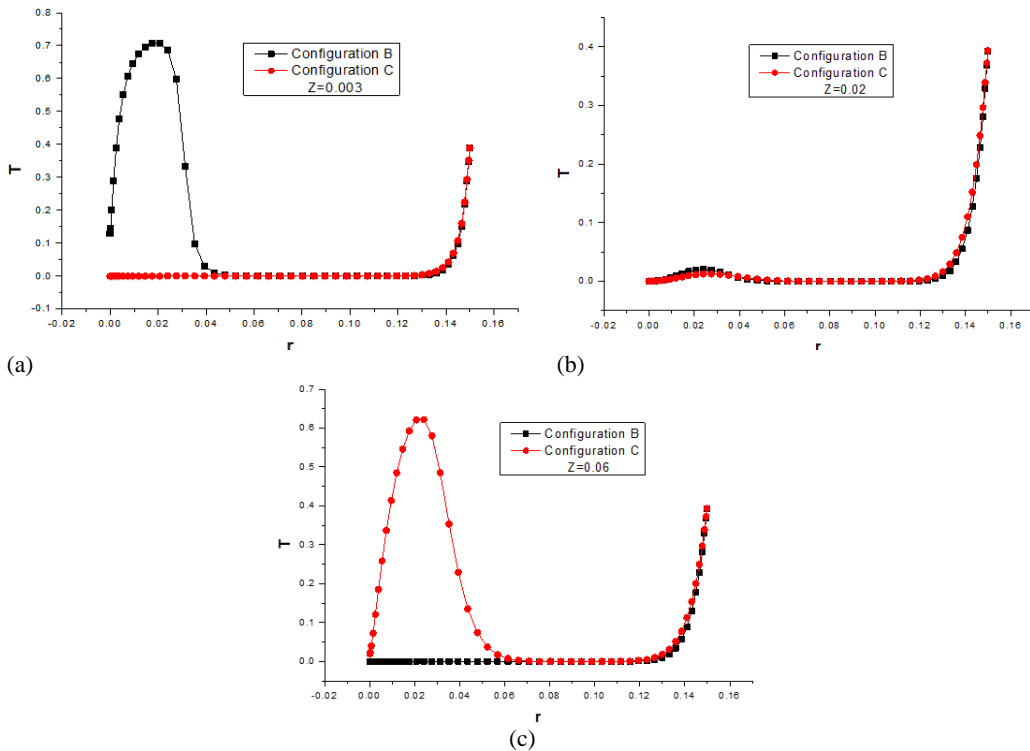


Fig. 37. Comparison of the T versus r in configurations B and C.

6. CONCLUSION

In the present investigation, a numerical study of laminar and turbulent natural convection flow generated with and without a hot obstacle was performed in a vertical cylindrical channel using

Fortran code based on the finite volume method. Measurements of the thermal and dynamic flows were conducted to validate the CFD code. The numerical results have been compared with our experimental results, and with other studies which show an excellent agreement in the general thermal and dynamical behavior of the flow.

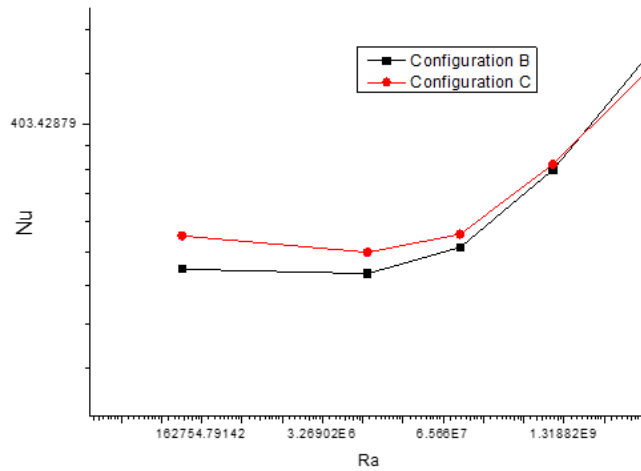


Fig. 38. Comparison of the Rayleigh number's impact on the Nusselt number in configuration B and C

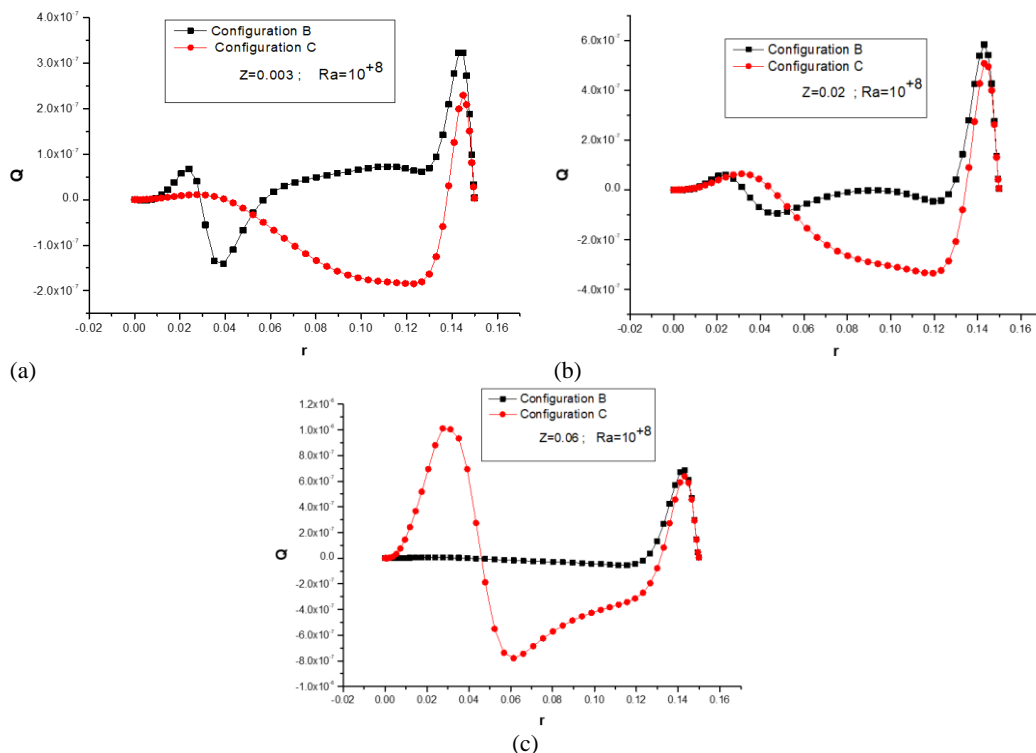


Fig. 39. Comparison of the Q versus r in configurations B and C

In the flow without the obstacle, the established regime appears at a form factor of $A=0.05$, whereas the boundary-layer regime is obtained at a form factor of $A=0.3$. The transition between the two regimes appears at $A=0.1$, which represents the critical regime. The effects of Rayleigh number and hot-obstacle location on the flow field were investigated.

The introduction of the hot obstacle in different positions did not affect the appearance of the flow regimes and particularly entailed the following.

- a noticeable improvement in heat transfer inside the cylinder.
- an intensification of the volume flow

REFERENCES

- Al Arbi, M., M. khamis and M. Abdulaziz (1991). Heat transfer by natural convection from the inside surface of a uniformly heated tube of different angles of inclination. *International Journal Heat Mass Transfer* 34(4-5), 1019-1025.
- Davis, L. P. and Perona, J. I. (1971). Development of free convection flow of a gas in a heated vertical open tube. *International Journal of Heat and Mass Transfer* 14(7), 889-903.
- Fujii, T., S. Koyama and V. K. Grag (1992). Transient natural convection over a heat generating vertical cylinder, *International Journal of Heat and Mass Transfer* 35(5),1293-1306.

- Garnier, C. (2015). *Modélisation Numérique des Ecoulements Ouverts de Convection Naturelle au Sein D'un Canal Vertical Asymétriquement Chauffé*. Ph. D. thesis, Pierre et Marie Curie University, France.
- Kapjor, A., P. Durcansky and M. Vantuch (2020). Effect of heat source placement on natural convection from cylindrical surfaces. *Energies* 13(17).
- Le Quéré, P., S. Xin, E. Gadoin, O. Daube and L. Tuckerman (2004). Recent progress in the determination of hydrodynamic instabilities of natural convection flows, In *Proceedings of CHT-04, ICHMT: International Symposium on Advances in Computational Heat Transfer*, Norway, CHT-04-K4.
- Maad, R. B. (1995). *Etude d'un Ecoulement de Convection Naturelle Dans un Canal Vertical Chauffé*, PhD thesis, Faculty of Sciences of Tunis.
- Maad, R. B. and A. Belghuith (1989). Méthode numérique de calcul du débit d'écoulement d'air par convection naturelle dans un canal vertical et confrontation expérimentale, 4ème Journées Internationales de Thermique, *Algerie*.
- Mahmoud, A. M. and Z. Yahya (2019). Improvement in the Performance of a Solar Hot Air Generator Using a Circular Cone. *International Review of Mechanical Engineering* 13(8).
- Mahmoud, A. O. M. (1998). *Etude de l'interaction d'un Panache Thermique à Symétrie Axiale Avec un Ecoulement de Thermosiphon*, PhD thesis, Faculty of Sciences of Tunis, El Manar University, Tunisia.
- Martin, L., G. D. Raithby and M. M. Yovanovich (1991). On the low rayleigh number asymptote for natural convection through an isothermal, parallel-plate channel. *Journal of Heat Transfer* 113(4), 899–905.
- Marzougui, M., L. Boutas and J. Zinoubi (2022), Thermal performance of nanofluids in rectangular microchannel with vortex generators: Application of electronic components cooling, In *International Energy Conference n 354 (E3S Web Conf.)*, 01008.
- Naffouti, T., L. Thamri and J. Zinoubi (2018). On the experimental analysis of the heating effect of open channel on thermal and dynamic characteristics of resulting flow plume thermosiphon. *American Journal of Engineering Research* 7(5), 89-106.
- Naffouti, T., J. Zinoubi and R. B. Maad (2010). Experimental characterization of a free thermal plume and in interaction with its material environment. *Applied Thermal Engineering* 30, 1632-1643.
- Naffouti, T., J. Zinoubi and R. B. Maad (2016). On the effect of aspect ratio of open heated channel including an active obstacle upon the turbulent characteristics of a thermal plume: experimental analysis. *Journal of Applied Fluid Mechanics* 9 (6), 3061-3071.
- Nakagome, H. and M. Hirata (1976). *The Structure of Turbulent Diffusion in an Axisymmetrical Plume*, *Ichmt*. Dubrovnik.
- Pantokratoras, A. (2006). Fully developed laminar free convection with variable thermophysical properties between two open-ended vertical parallel plates heated asymmetrically with large temperature differences. *Journal of Heat Transfer* 128(4), 405–408.
- Rouse, H., C. S. Yih and H. W. Humphreys (1952). Gravitational convection from a boundary source. *Tellus* 4(3), 201-210.
- Terekhov, V. I., A. L. Ekaid and K. F. Yassin (2016). Laminar free convection heat transfer between vertical isothermal plates. *Journal of Engineering Thermophysics* 25(4), 509-519.
- Vorayos, N. (2000). *Laminar Natural Convection Within Long Vertical Uniformly Heated Parallel Plate Channel and Circular Tubes*, Ph. D. thesis. in mechanical Engineering, Oregon State University.